STUDY OF COOLING STRATEGIES FOR METAL PROFILES THROUGH FINITE ELEMENT MODELS

Alpha Pernía Espinoza [ap], Fco. Javier Martínez de Pisón Ascacíbar [a], Manuel Castejón Limas [b], Ana González Marcos [b]

[a] Universidad de La Rioja, c/ Luis de Ulloa 20, 26004, Logroño-La Rioja, Spain. Phone +34 941299232. Fax +34 941299794

[b] Universidad de León, Campus de Vegazana, s/n, 24071, León-Castilla y León, Spain. Phone +34 987291000 - Ext. 5382. Fax +34 987291790

e-mails: {alpha-veronica.pernia, fjmartin}@dim.unirioja.es; {manuel.castejon, dieago}@unileon.es

ABSTRACT

The present paper studies the behaviour of metal profiles during different cooling configurations through finite element models. These models include the contact with the supporting table and the effect of the weight of the beam. The analysis presented provides a computational technique for predicting the residual stress and deflection of metal profiles within acceptable accuracy.

KEYWORDS: Cooling Bed; Thermal Bending; Advanced Simulation; FEM; Process Plant.

1. Introduction

We present the development of a Finite Element Model (FEM) for the cooling of HE- beams. These profiles have constant cross-sectional geometries but different parts of the cross-sections have different thickness. Such asymmetries lead to non-uniform cooling. In addition, accelerated cooling systems (as water sprayed lines) contribute to the non-uniform cooling and, as a result, to the development of thermal stresses, which may be higher than the yield stress of the material at high temperatures. The situation leads to bending of the beam and development of residual stresses. In some cases, the thermal deflections are larger than the maximum opening of the roller straightener (which is a process that follows the cooling of the profiles) and the deflected beam cannot be straightened. Then, to facilitate the straightening process (i.e. to reduce process time and costs) and improve product quality, reduction of the thermal bending is very important. The FEM model created here could make possible the study of superficial and internal (cross section) temperatures and stresses during the cooling of the beams, helping the design of cooling strategies to reduce bending and residual stresses. The software selected for the simulation was ABAQUS®. ABAQUS® is a powerful tool that has the capability for coupled and decoupling mechanical and thermal solving problem.

Notation

c	specific heat [J/kg ºC]
E	elastic modulus [Pa]
e_m	emisivity
g	acceleration due to gravity = 9,81 m/s^2
h_f	film heat transfer coefficient [W/m^2 ºC]
k	thermal conductivity [W/m ºC]
α	coefficient of linear thermal expansion [ºC^{-1}]
ρ	density [Kg/m^3]
v	Poisson's ratio

σ_y yield stress [Pa]
S-B Stefan-Boltzmann constant = 0.567e-8 W/m^2K^4
W flow rate of cooling water $[m^3/(s\ m^2)]$

2. Problem Definition

2.1. Section simulated

We have simulated the cooling of the HEA450 profile, in still air and, subsequently, in the presence of water spray lines on the cooling bed. The FEM model obtained could be easily adapted to other beam sections.

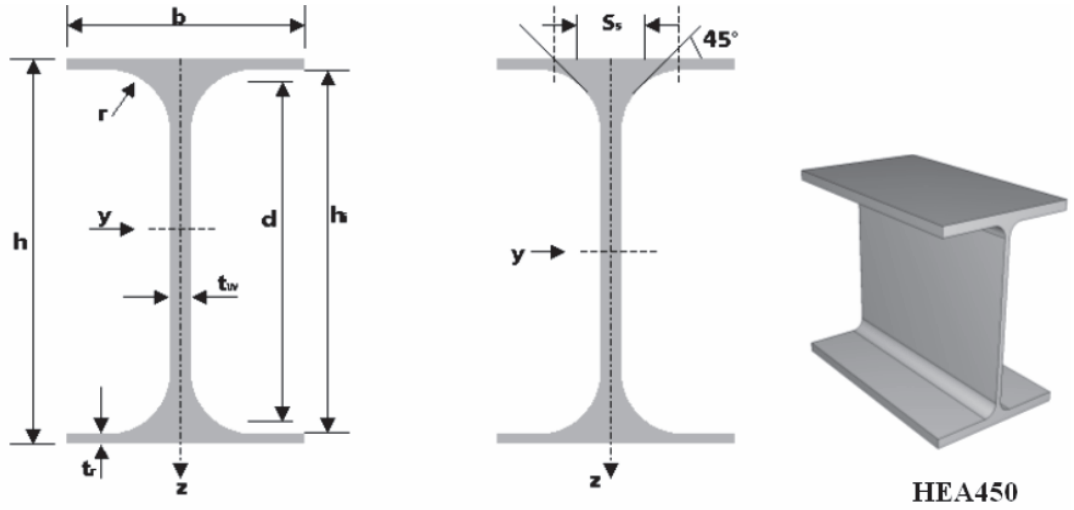

SECTION	h	b	t_w	t_f	r
HEA450	440	300	11.5	21	27

Figure 1. HEA450 dimensions and ABAQUS's part.

2.2. Mechanical and Thermal Properties

The material thermal and mechanical properties considered for the simulation are presented in the next table.

Table 1. HEA450 material mechanical-thermal properties.

Temperature (ºC)	**30**	**200**	**350**	**600**	**850**	**950**
E (GPa)	210	180	160	140	130	50
v	0,30	0,26	0,23	0,13	0,12	0,12
σ_y (MPa)	35,0	33,0	28,5	5,5	1,0	0,5
ρ (kg/m^3)	7850	7850	7850	7850	7850	7850
α x 10^{-5} $(ºC^{-1})$	1,10	1,15	1,31	1,40	1,50	1,50
k (W/mºC)	48,1	45,2	38,1	32,7	24,4	16,0
c (J/kg ºC)	490	540	607	712	830	920
e_m	0,8	0,8	0,8	0,8	0,8	0,8

2.3 The Cooling Bed

After the hot rolling, the rolled products move, through the ingoing roller table (consisting of carbon steel rolls, equally spaced), to the cooling bed which is a framework of equally spaced carbon steel beams parallel to each other.

Figure 1 presents a diagram of the cooling bed considered.

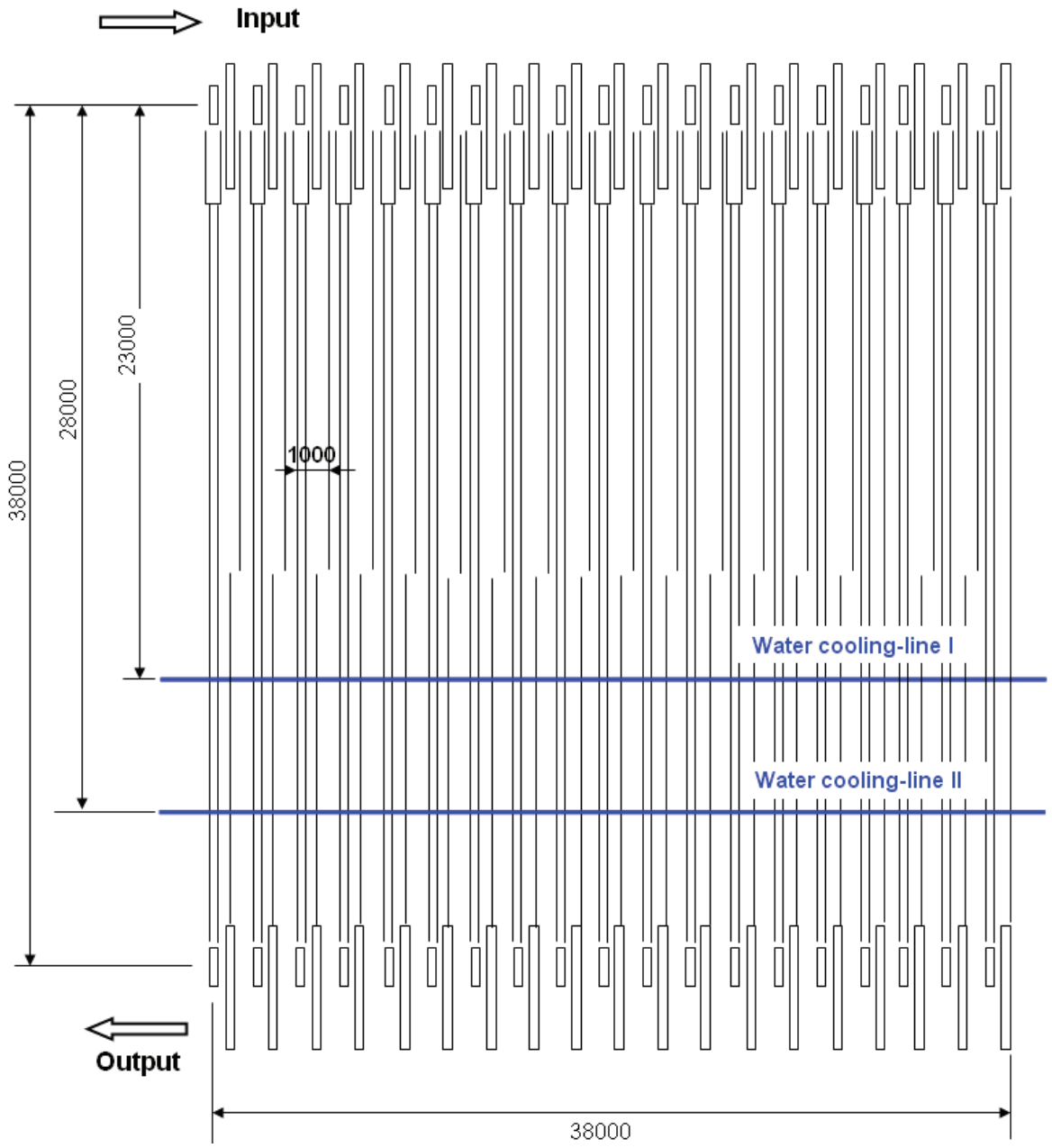

Figure 2.Configuration of the Outdoor Walking Beam Cooling Bed considered.

It has an accelerated cooling system based on water spraying on the bottom and top of the beams (the flanges' external surfaces). There are two water cooling lines (represented by the blue lines in Figure 2.

The following table resumes the main dimensions and time parameters of the cooling bed.

Table 2. Parameters of the Cooling Bed

PARAMETER	VALUE	UNIT
Total length	38000	mm
Total width	38000	mm
Distance between the skids of the fixed beams	1000	mm
Water Cooling Line I (distance from input)	23000	mm
Water Cooling Line II (distance from input)	28000	mm
Input temperature	600-950	ºC
Output temperature	20-120	ºC
Cooling total time	46-55	min
Step width	850	mm
Time between two steps (idle time)	74	s

We can state that the beam is cooled in five phases:

- **First**: the beam is set by the ingoing roller table in the cooling bed, and starts its journey along it. For about 30 minutes is cooled only by air.
- **Second**: the beam reaches the first accelerated cooling system, the Water Line I, and is cooled by sprayed water (from below and above) for about 6 minutes.
- **Third**: the beam leaves the water system and, still wet, moves into the second water system, for approximately 2 minutes.
- **Fourth**: the beam arrives at the Water Cooling Line II, and is cooled again by sprayed water (from below and above) for about 6 minutes.
- **Fifth**: finally, the beam leaves the water system and moves in the still air for about 11 minutes, until it reaches the outgoing roller table.

The times periods established here are approximations according to a total cooling time of 55 minutes.

3. The Fem Models

The cooling of the HEA450 beam was modelled with ABAQUS/Standard in a sequentially coupled thermal-stress analysis. The sequential analysis was used because the stress/deformation field in the beam depends on the temperature field in the beam, but the temperature field is not significantly affected by the stress/deformation response. The beam cooling was possible through heat transfer to the ambient and the water sprayed using convection and radiation.

We modelled the beam by a FEM with elements C3D8T (an 8-node thermally coupled brick, trilinear displacement and temperature). The mesh of the cross section is shown in Figure 3. The element length in beam direction was established in 100mm.

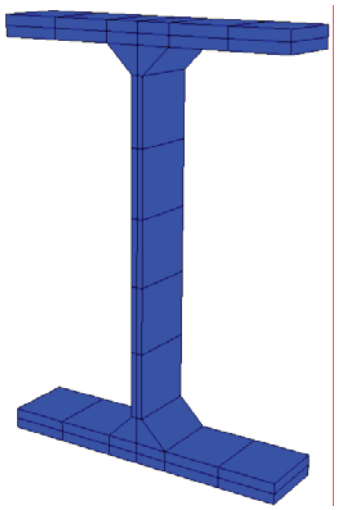

Figure 3. Beam HEA450 FEM mesh

The beam length modelled was 8 m, and it was supported by nine bars, separated 1m from each other (Figure 4). It is important to point out that the model obtained can be easily adapted to a longer or shorter beam. We use this length because it is long enough to represent the different thermal and mechanical situation along the beam and at the same time it is still computationally efficient.

The supports were simulated as analytical rigid extruded shell with dimension: 0,15m width x 2m length x 0,02m height. The contact pair beam-supports was simulated with a Coulomb friction coefficient of 0,1. We have also included the effect of gravity forces over the beam (9,81 m/s^2).

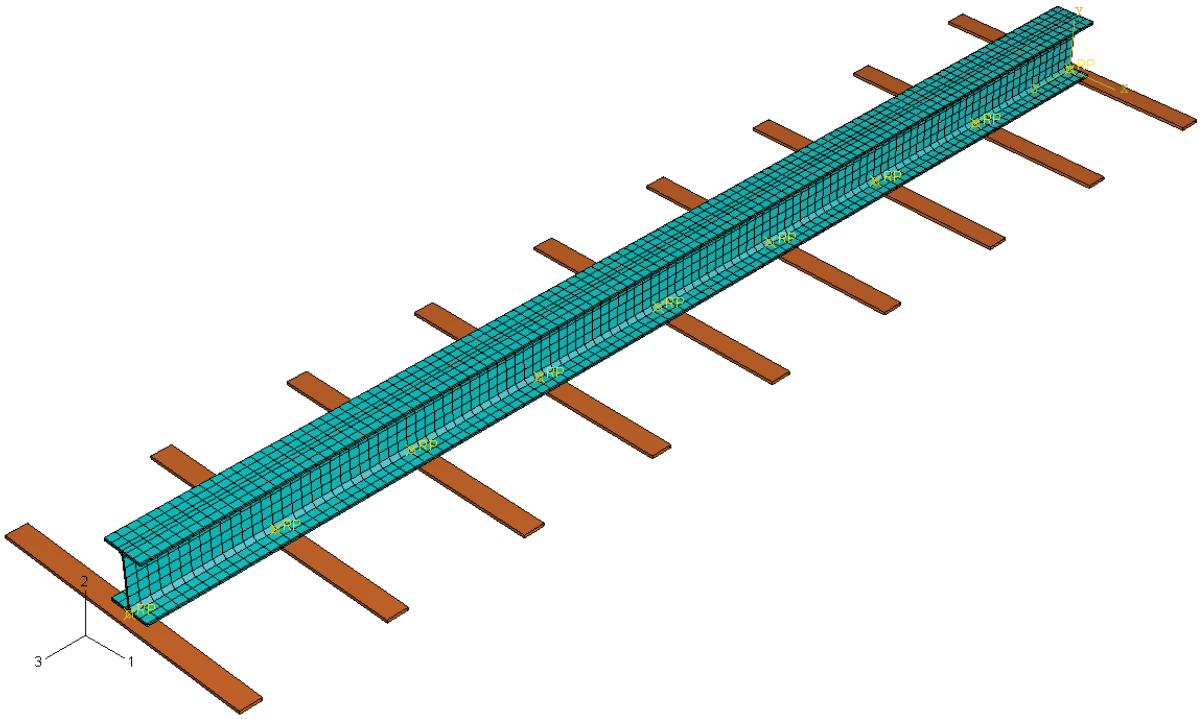

Figure 4. Cooling bed FEM. Beam mesh.

We assumed the following values for the simulation:

- Input beam temperature: 950 ºC
- Ambient temperature: 20 ºC.
- Stefan-Boltzmann radiation constant: 5,6697e-8 W/m^2K^4 [Basu et. al, 2004].
- The film coefficient (*h*), representing the convection, was modelled by the function showed in Figure 5 for the different phases of the cooling bed (values based in [Basu et. al, 2004]). At the beginning (Phase 1) the beam is cooled only by air, with a low film coefficient (6,5 $W/m^2ºC$). Next, the water from the Water Line I start to fall over the beam surface, until it reaches to a maximum (when the beam is behind the Water Line I), represented by a film coefficient of 800 $W/m^2ºC$ (Phase 2). After some minutes the beam moves away from the first water line and the *h* decreases, until the beam starts to approximate to the second water line (Phase 3), when the pattern is repeated (Phase 4 and 5).

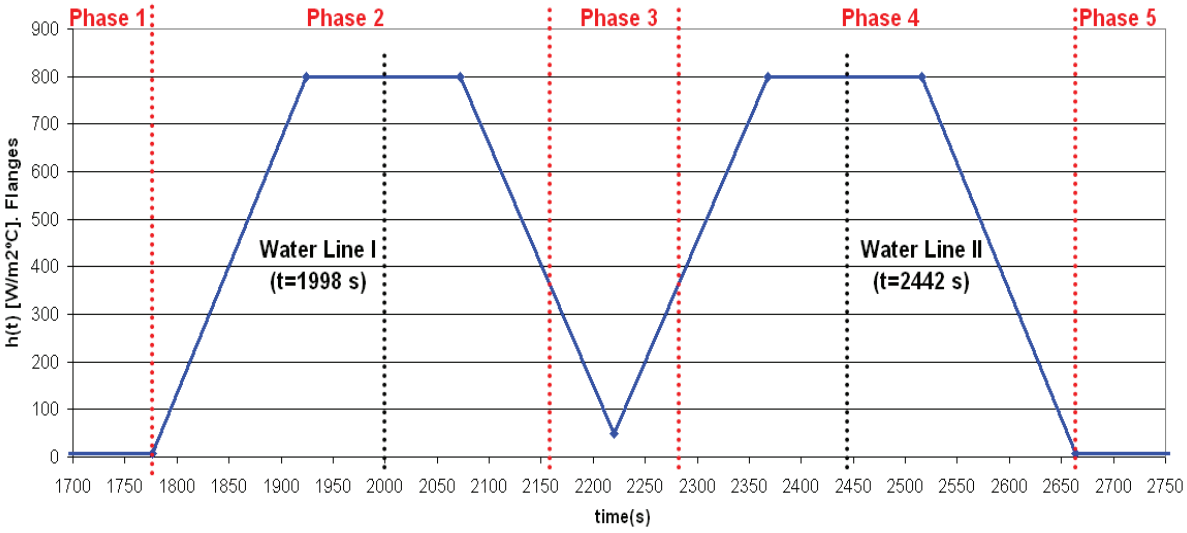

Figure 5. Film coefficient between the beam and surroundings

As it is logical, the water is sprayed first at the front part of the flange (line "*a*", in Figure 6), and then, as the beam moves forwards to the water line, the water reaches the back part of the flange surface (line "*b*"). This is represented by repeating the same *h* function at the back line of the beam (*b*). In between, the *h* is interpolated linearly, as can be seen in the same figure (Figure 6).

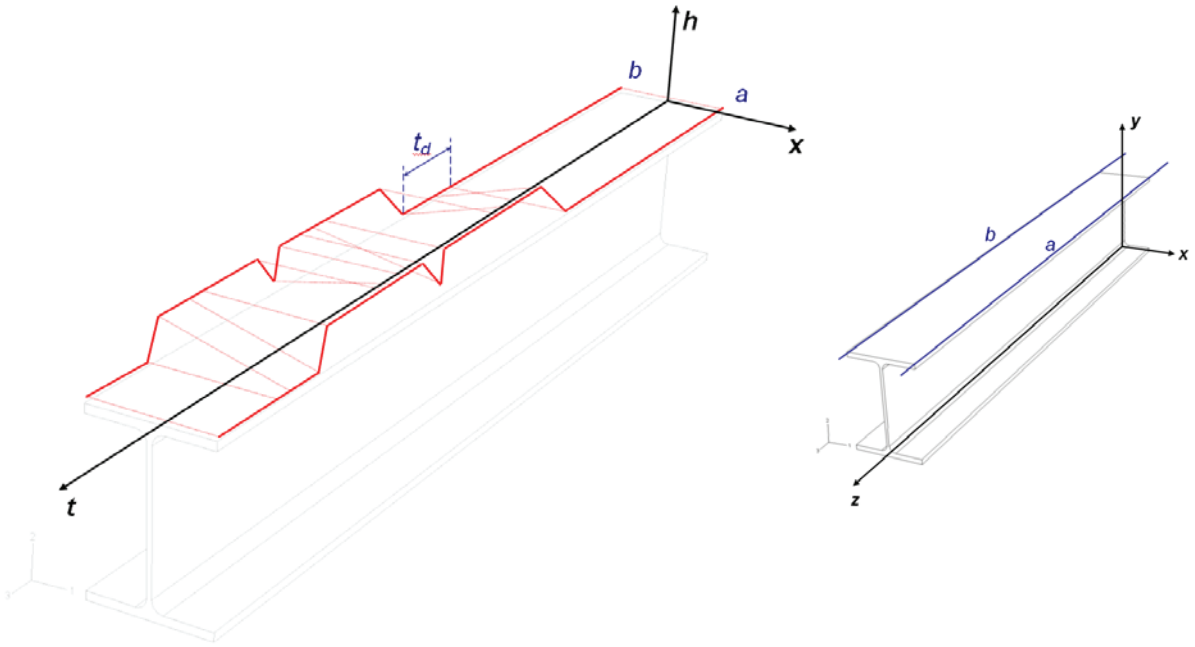

Figure 6. Film coefficient at the flange surface as a function of time (t) and x dimension.
"td" is the delay time between the arrival of the h function from line "a" to line "b". See annex 1 fro details.

Similarly, for the rest of the beam surface (web, roots and rest of flange's surfaces) the film coefficient increases when the beam moves forward the Water Lines I or II, and decreases when it moves away from them.

4. Results

In this section we present the results obtained from the thermal and stress/displacement simulations.

Temperature history during cooling is shown in the next page (Figure 7). Point 1 represents the center of the flange surface (TF 1), point 2 represents the center of the web surface (TW 2) and point 3 represents the root surface (TR 3). These results are compared with experimental values (TF 1E, TW 2E, TR 3E).

It can be seen from Figure 7, that the temperature history obtained from the simulation is very similar to the obtained in the experimental test. The simulation presents similar cooling rates and temperature values.

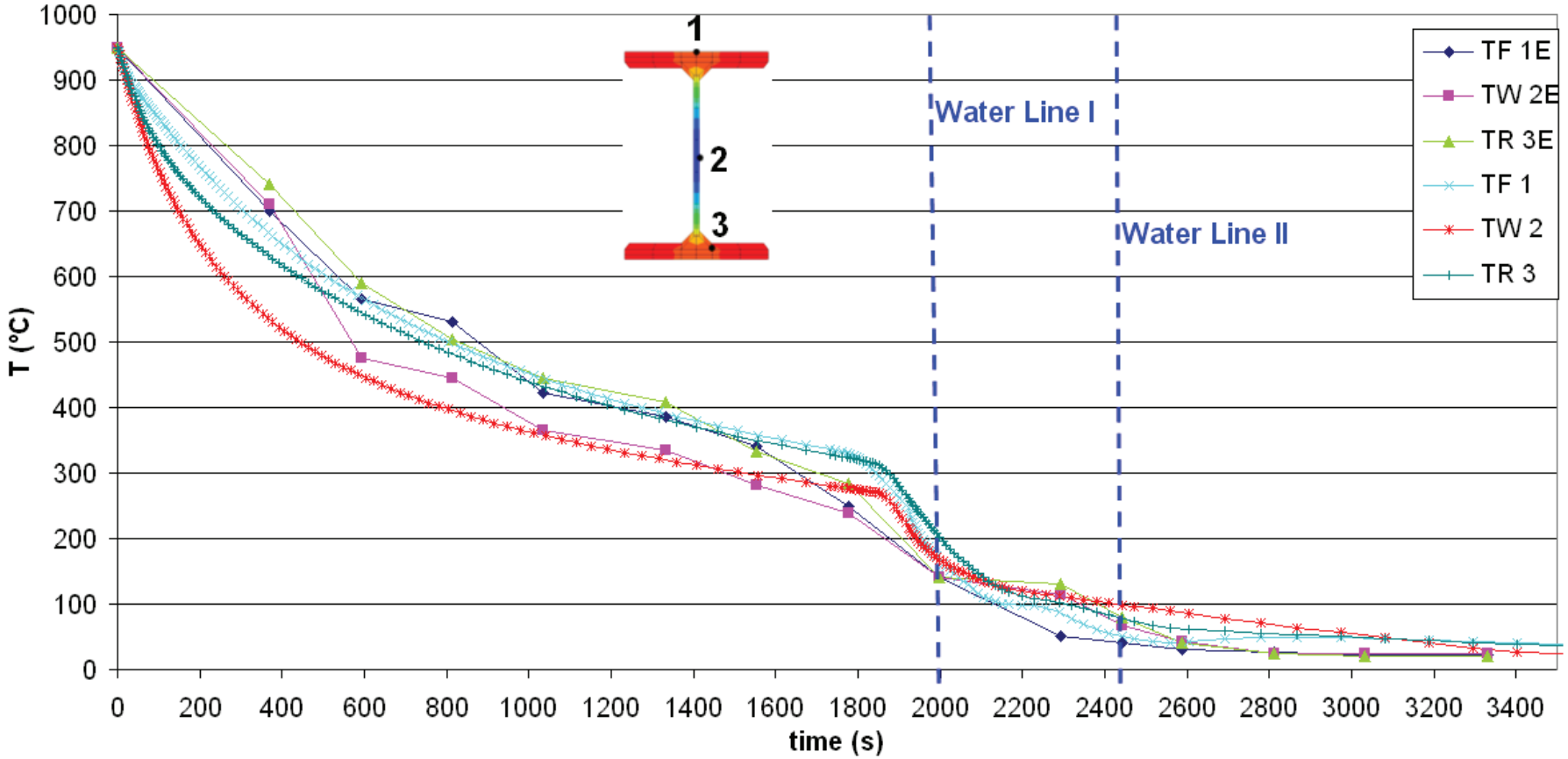

Figure 7. Temperature history in the middle cross section of the beam.
"TF 1E", "TW 2E", "TW 3E": Experimental Flange, Web and Root temperatures; "TF 1", TW 2", "TR 3": Simulated Flange, Web and Root temperatures.

Table 3. Simulation results.

Distance (m)	0	4	7	9	12	15	18	20	23	26	28	30	32	35	38
t (s)	0	370	592	814	1036	1332	1554	1776	1998	2294	2442	2590	2812	3034	3300
Flange (TF 1)	950	669	573	495	446	389	360	328	159	87	60	53	62	56	37
Root (TR 3)	950	634	549	479	433	379	352	321	185	102	86	72	63	54	33
Web (TW 2)	950	532	450	393	358	319	299	276	171	111	99	86	65	52	24

We can see that during Phase 1 and at the beginning of Phase 2, the web (2) cools down faster than the rest of the beam points, followed by the root (3) and the flange (1). In Phase 2 the temperatures approach each others. In Phase 3 and 4 the web cools down slower than the root and flange. And finally, at the end of Phase 5, all temperatures seem to balance (towards the ambient temperature).

Figure 8 shows the temperature profile of the beam middle cross-section, at the end of the cooling bed (time: 55 min ≡ 3300 s). The temperature profile is very similar along the beam at this final time.

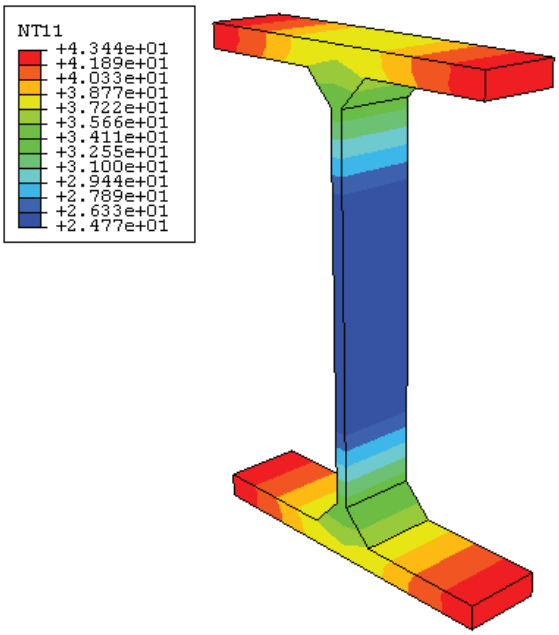

Figure 8. Beam center temperature contour plot at final time 55 min..

The flange extremes are the last to cool down, followed by the roots and the web.

However, there are several environmental variables, such as wind speed, ambient temperature, film coefficient of possible "double-face fluid" (water in contact to the hot beam), which have to be modelled in order to improve the simulation. This will be accomplished in the near future using CFD simulation, in particular, using FLUENT software. To achieve this, is necessary to count with more experimental tests, including data from the surroundings conditions (wind speed, ambient temperature, beams configuration on the cooling bed, etc).

During Phase 1 the beam cools down symmetrically (Figure 9).

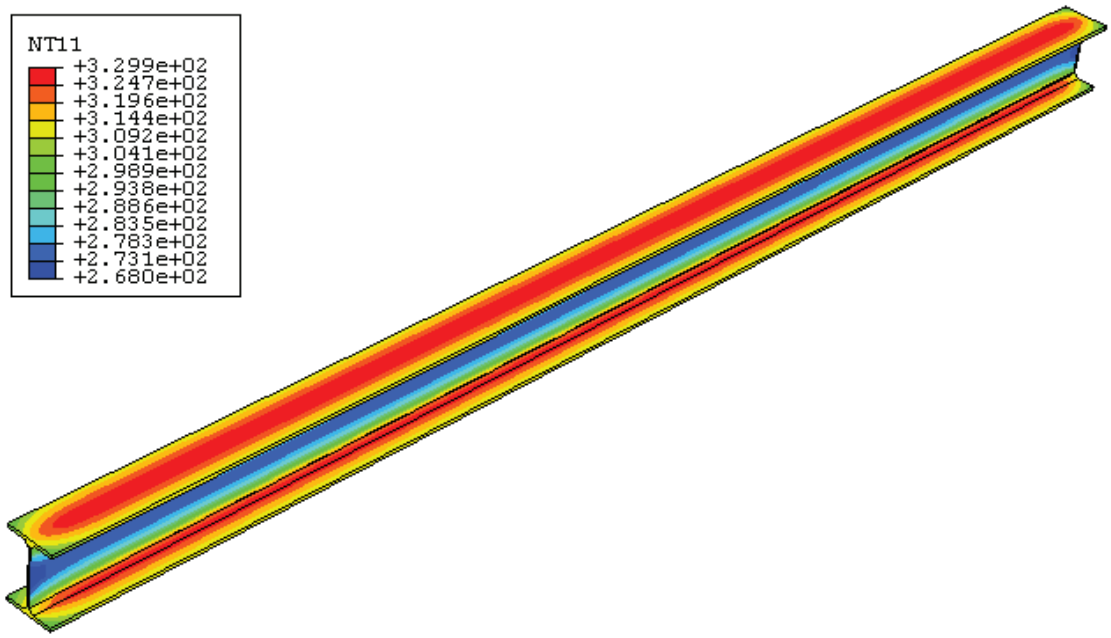

Figure 9. Beam temperature contour plot at final time of Phase 1 (1772 s).

Nevertheless, when it moves near the Water Line I (at time 1776 s) and, further, the Water Line II (at time 2220s), the beam cools down asymmetrically. The front part of the beam cools down faster than the rest of the beam, as we can see in Figure 10: temperature contour plot at time 1895s (beam starts receiving water from Water Line I).

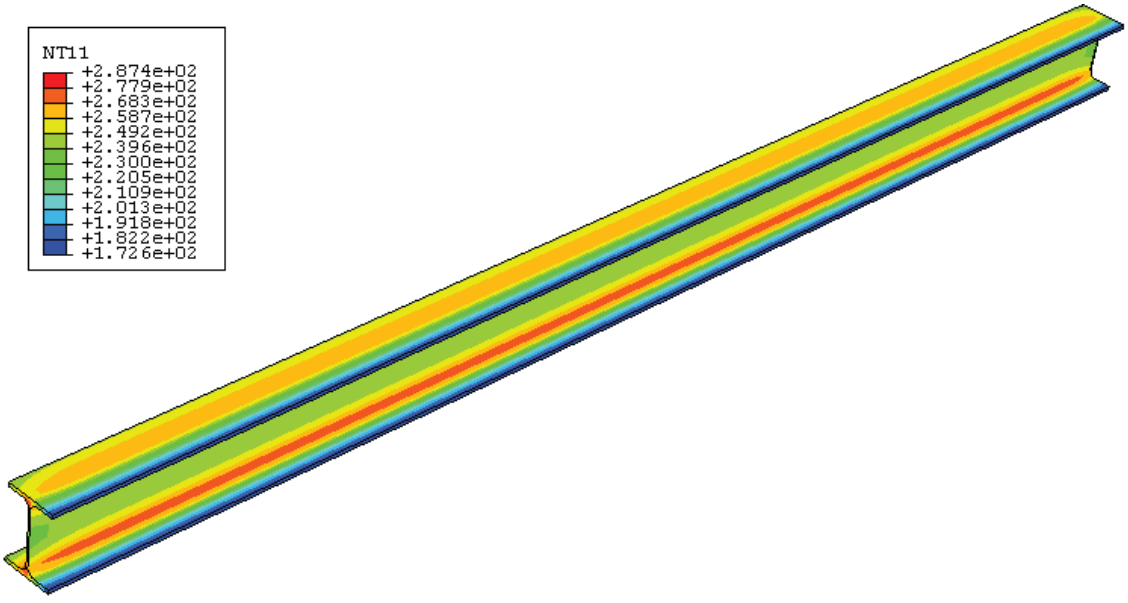

Figure 10. Beam temperature contour plot at the beginning part of Phase 2 (1895 s).

In the next figure we can see how the beam is cooled uniformly again, when it is located under WL I (t= 2070s).

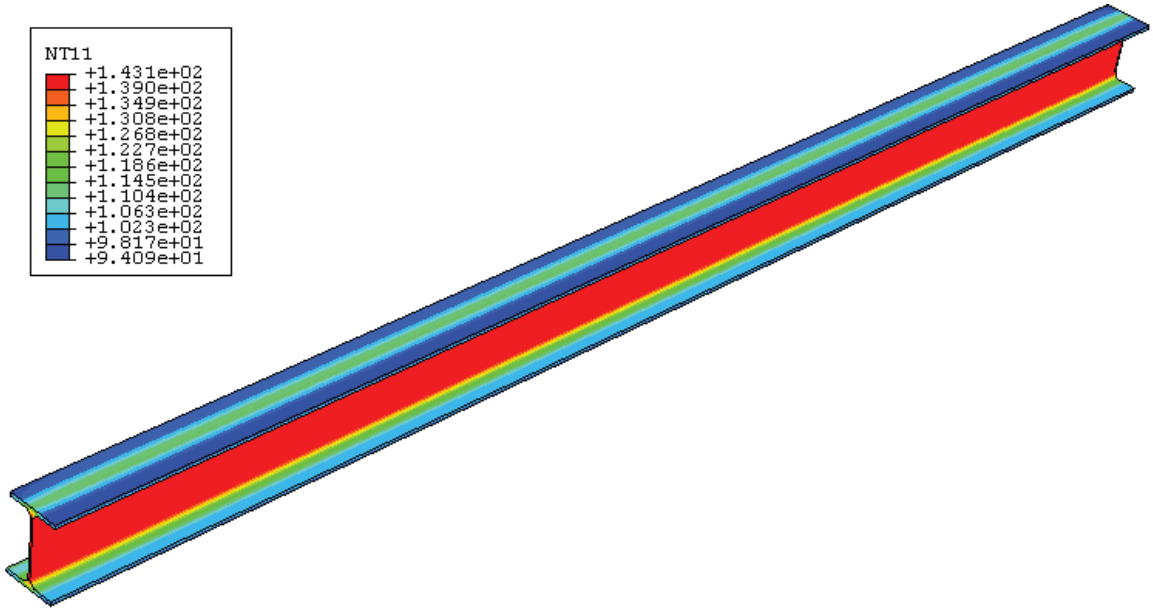

Figure 11. Beam temperature contour plot, at Phase 2, at time 2070 s.

In Figure 12 the beam's temperature contour plot at the beginning part of the Phase 3 is presented. As in Figure 10, the beam's front part present a lower temperature compared to the rest of the beam, but now the differences are smaller.

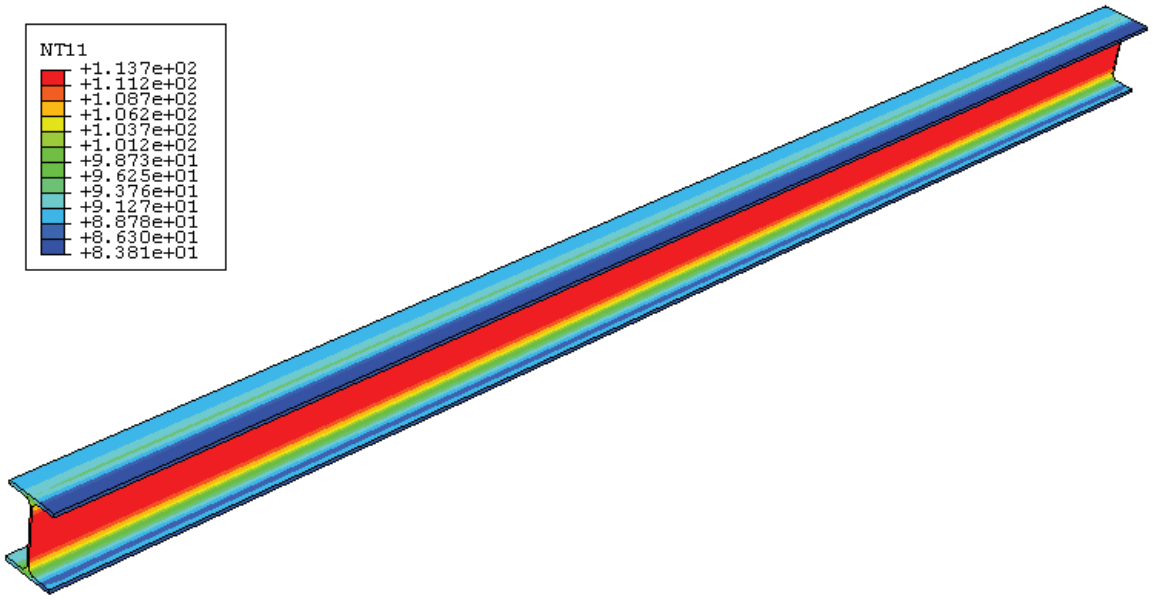

Figure 12. Beam temperature contour plot, at the beginning part of Phase 4, at time 2272 s.

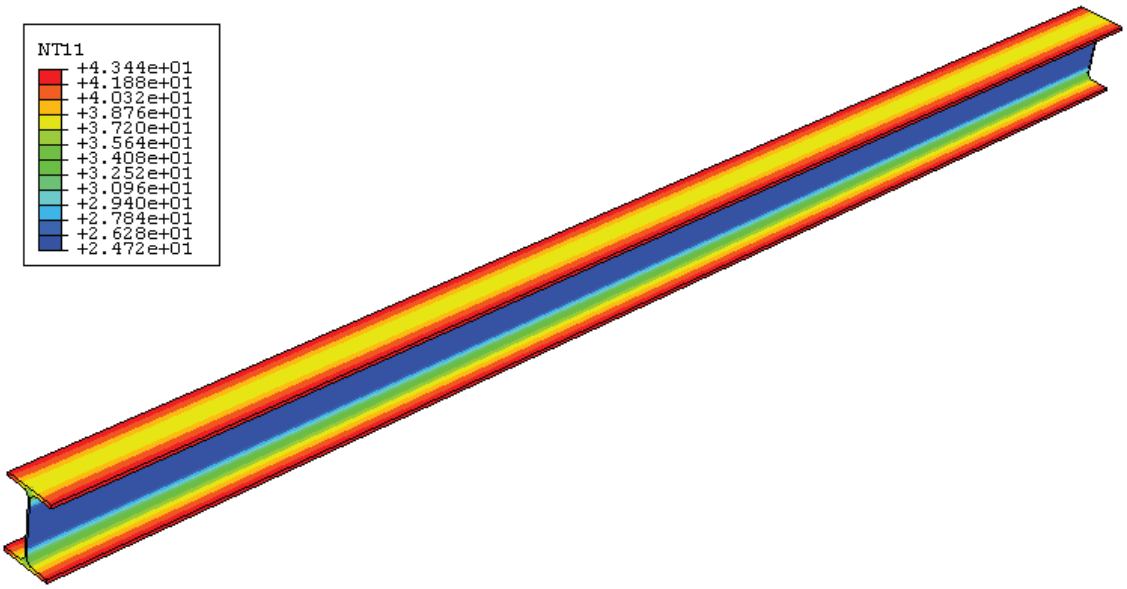

Figure 13. Beam temperature contour plot at the end of Phase 5, at time 55 min (3300 s).

This situations, added to the differences in thickness of beam HEA450 section, leads to the **bending** of the beam in the *xz* plane.

We define the beam camber as in Figure 14. The positive camber corresponds with the beam moving direction on the cooling bed.

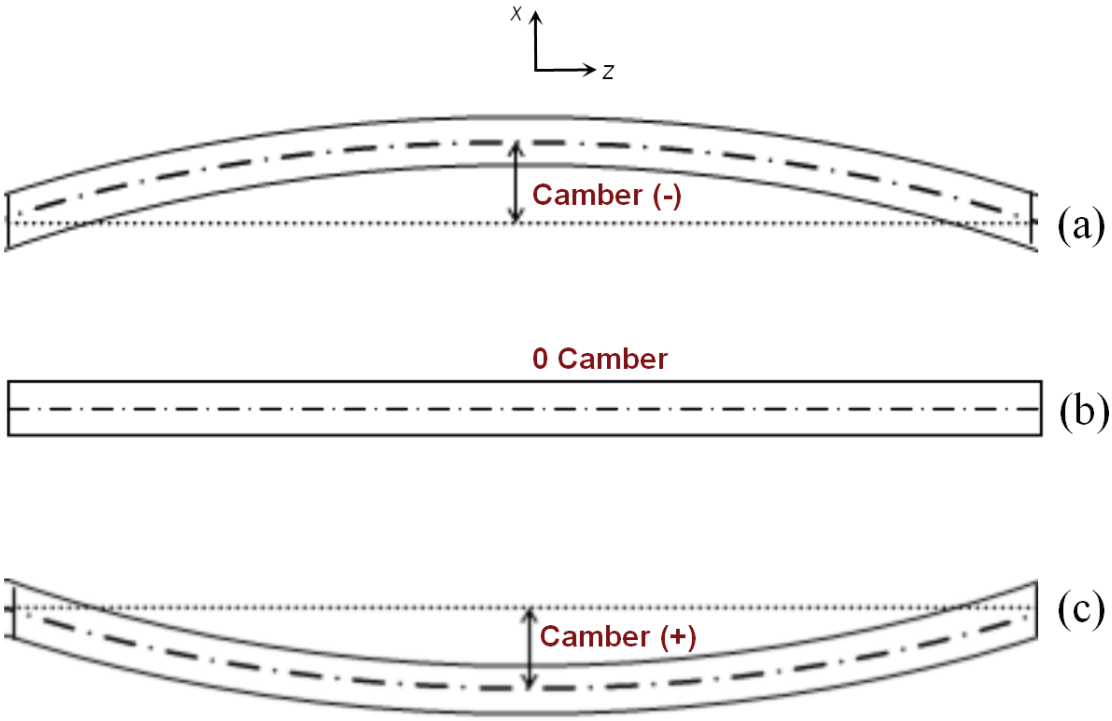

Figure 14. Definition of beam camber.

In Figure 15 the bending evolution of the beam obtained from the FEM, in the *xz* plane, is presented.

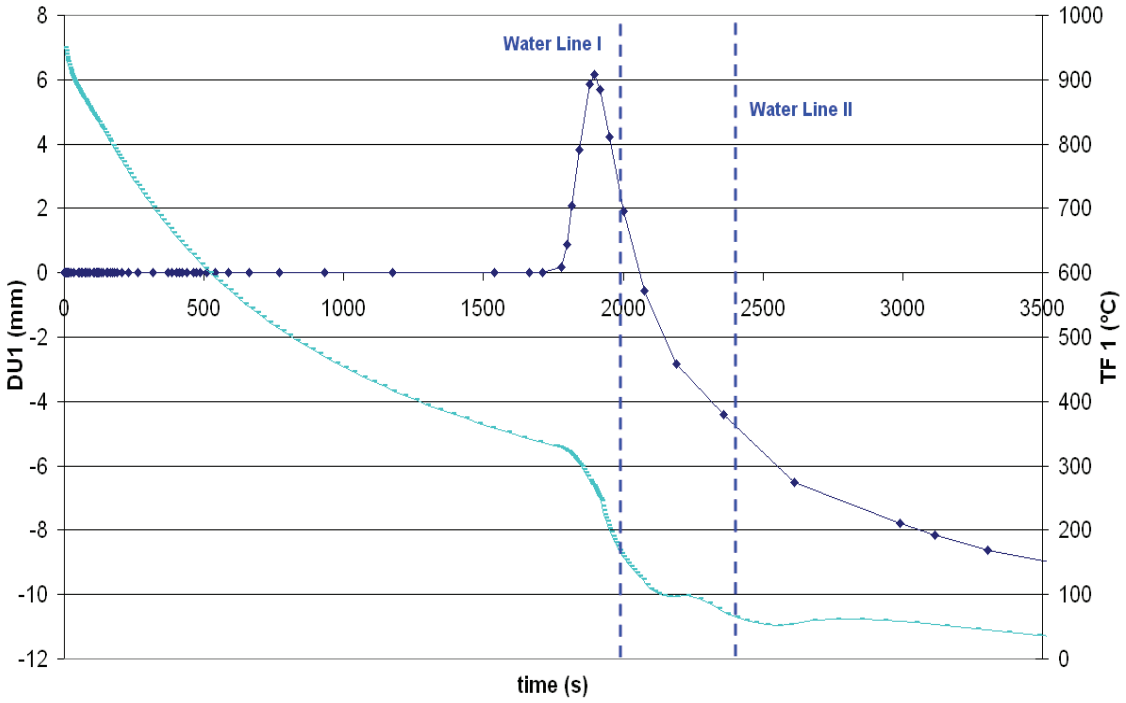

Figure 15. History of beam camber and, as a reference, flange center node temperature evolution (TF 1)

It can be seen that when the beam reaches the Water Line I (WLI) it starts to bend in the *x* positive direction. This can be explained because of the contraction of the beam's front part, which reaches first the water sprayed (see Figure 10). The bend reaches its maximum, equal to 6,15 mm, at *t*=1895 s (31,6 min). Then, at time 2070 s (34,5 min), the entire beam is under WL I and the beam cools down uniformly (see Figure 11). As a result the beam gets straight again (camber = 0 mm). Immediately, as the beam moves towards the beginning part of Phase 3, it starts to comb in the negative direction, because the back part of the beam cools down faster than the front part, and contracts the beam in that direction. Under WL II the temperature difference is reduced. In the end, at the final time 3300 s (55 min) the beam reaches a bending of -8,6 mm, and the tendency is a bend of -9,5 mm, reached at 5000 s (83 min). This bending evolution has to be confirmed with experimental tests.

The **stress** evolution of points (flange, web and root) studied before is presented in the next figures.

Flange center (F-1) principal component stresses (S11, S22 and S33) along the time are depicted in Figure 16.

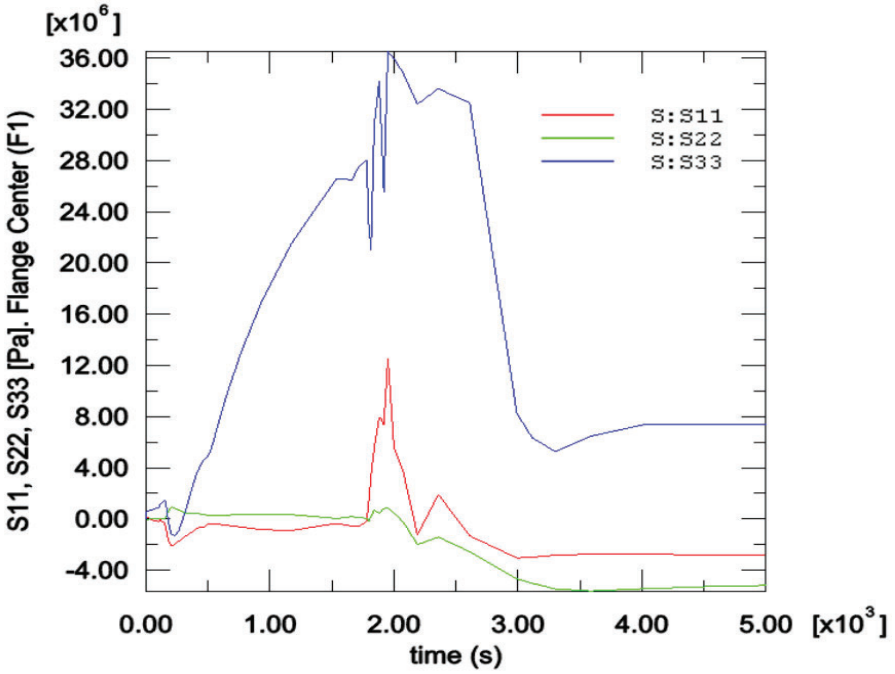

Figure 16. Stress principal components history of flange center node (F-1)

Comparing the three stress components (S11, S22 and S33), the longitudinal stress (S33) is the dominant stress in this process, with values more significant than the rest of the components (S11 and S22). Therefore, we will focus the analysis on the longitudinal stresses, S33.

In the next figures we show the longitudinal stress (S33), the temperatures (T) and the yield stress (Sy or σy) of the Flange (F-1), Web (W-2) and Root (R-3) points.

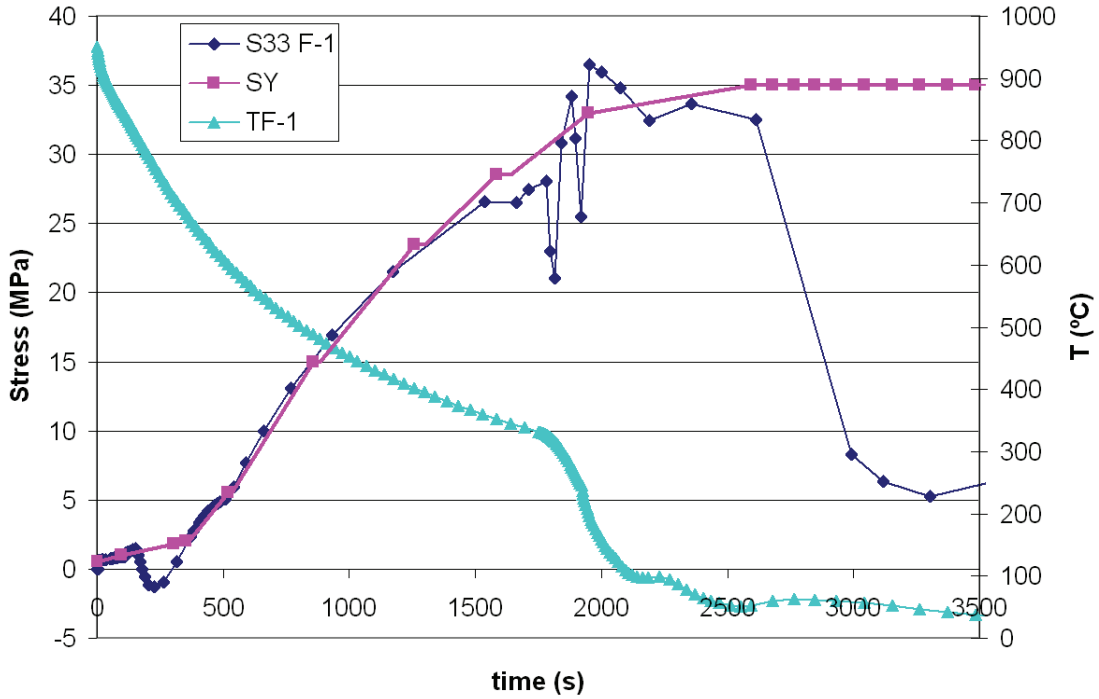

Figure 17. S33, Sy and TF-1, of flange center node.

In Figure 17 (flange behaviour), the S33 exceed the yield stress at 1895 s, when the beam present the maximum positive bending (Figure 15). And also Sy is exceeded at 1951 s, when the beam is under Water Line I.

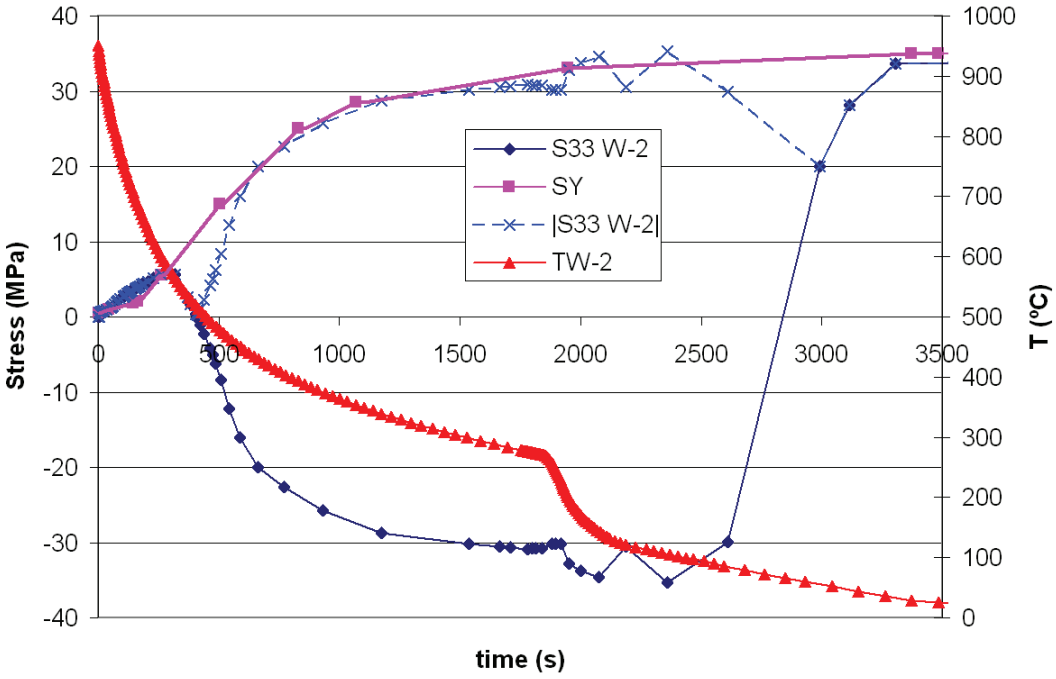

Figure 18. S33, Sy and TW-2, of web center node.

In Figure 18 (web behaviour), the Sy is exceeded twice: at 2070 s, when the beam gets straight again; and at 2360 s when it starts to comb in the negative direction.

We can observe that there are several situations in which the longitudinal stress (S33) is higher than the yield stress (Sy). This leads to plastic deformation, and the subsequent partial (elastic) and permanent (plastic) bending of the beam.

All these results have to be verified by experimental test.

The longitudinal **residual stress** (S33) of the beam after cooling (time 55 min) is depicted in the following figure.

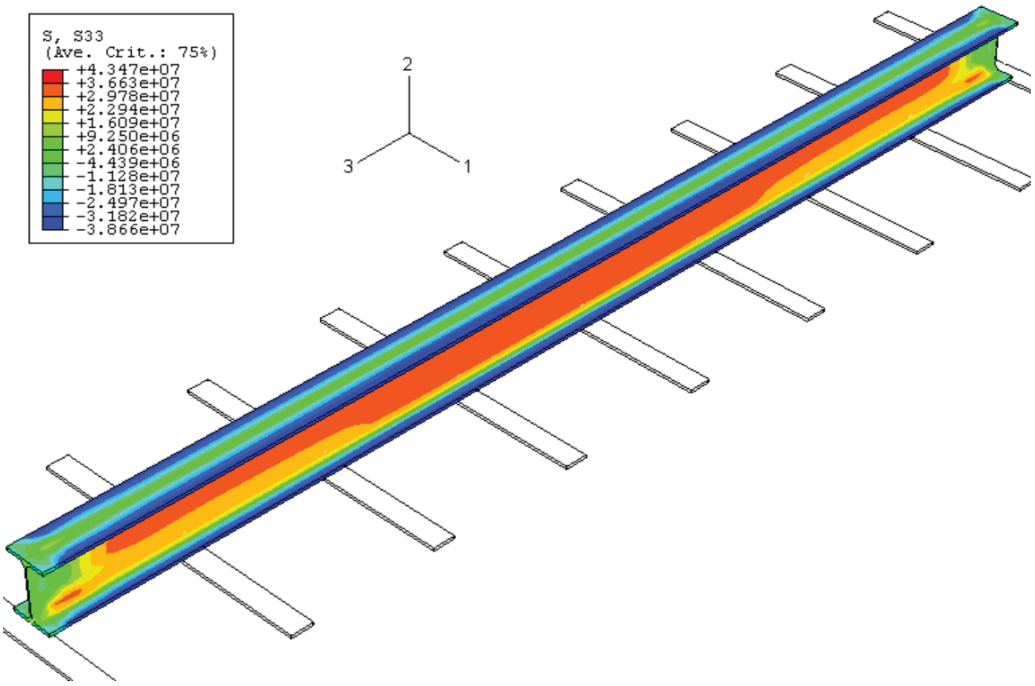

Figure 19. Beam "front part" residual stresses contour plot [Pa]. At time 55 min

The beam residual stresses vary depending on the side ("front" or "back" side), causing the permanent bending (-8,6 mm). And it also varies from edge to center. The higher stresses are located at the beam center, with tensile stresses at the web and compressive stresses at the flange extremes.

The unstraightened beam has tensile residual stresses at the web and roots (with a maximum of +43,47 MPa at the web and 29,78 MPa at the roots); and tensile residual stresses at the flange extremes -38,66 MPa. However, we have to verify these results with experimental tests.

In the next figure there is a perspective view, in which one can perceives the final bending of the beam (time: 55 min).

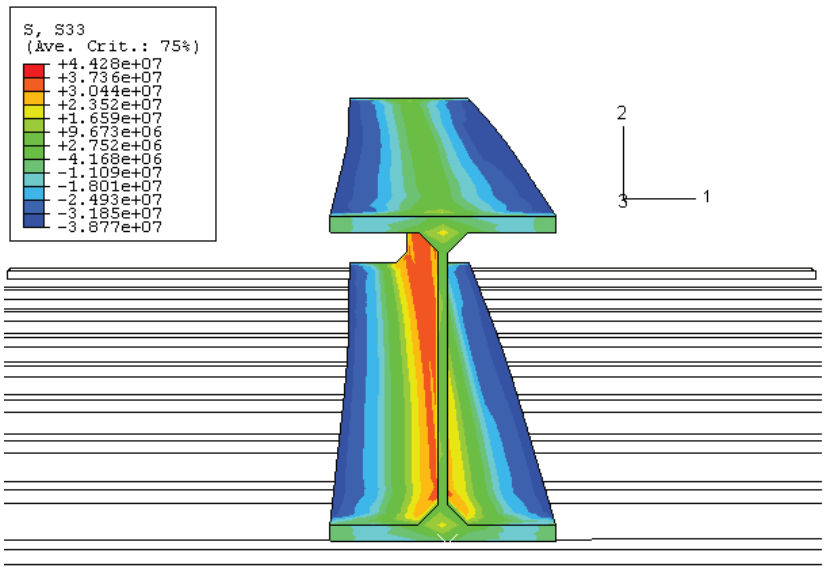

Figure 20. View of the final bending of the beam (at time= 55 min).

5. Conclusions

We have presented a Finite Element Model (FEM) representative of the cooling of the beam in the cooling bed. The temperature profiles obtained through the model are in concordance with the experimental tests and results showed in literature. Nevertheless, we have to verify the bending results and the residual stresses with experimental values. In addition, we have to complete the study of the beam cooling with CFD (Computational Fluid Dynamics) simulations, including wind speed, ambient temperature variation, film coefficient of possible "double-face fluid", in order to obtain a more realistic representation of the cooling bed.

6. Acknowledgements

We would like to thank the valuable collaboration of Peiner Träger GmbH, in particular to Mr. Jens Eicke for assisting us in the understanding of the process and give experimental data at our disposal. We are also very grateful to Mr. Joaquín Ordieres- Meré, from Universidad de La Rioja, for his priceless contribution.

This work has been supported by the European Union under the RFCS program references: RFS-CR-03012, RFS-CR-04023 and RFS-CR-04043; and the CEUTIC INTERREG IIIA program. It also has been partially funded by the Spanish Ministry of Education, Culture and Sport (MECD) and Ministry of Science and Technology by means of the "Dirección General de Investigación" project: DPI2004-07264-C02-01. We also want to recognize the support received from the "2º Plan Riojano de I+D+i" of the Government of La Rioja.

References

Abouaf M., Chenot J. L., Marcelin J. L. (1983), "A two-dimensional finite element idealization for thermo-elastic deflection in beams", *Int. J. Numer. Meth. Eng.*, 19, pp. 1453-1465.

Basu J., Srimani S. L., Gupta D. S. (2004), "Rail behaviour during cooling after hot rolling", *Journal of Strain Analysis for Engineering Design*, v.39, no.1, pp. 15.

Boyadjiev I.I., Thomson P.F., Lam Y.C. (1996), "Computation of the diffusional of continuously cooled austenite for predicting the coefficient of thermal expansion in the numerical analysis of thermal stress", *ISIJ Int.*, v. 36, no. 11, pp. 1413–1419.

Boyadjiev I.I., Thomson P.F., Lam Y.C. (2004a), "Prediction of the deflection and residual stress in controlled cooling of hot-rolled steel beams including load and arbitrary support. Part I. Computational model", *Journal of Material Processing Technology*, 147, pp. 370-376.

Boyadjiev I.I., Thomson P.F., Lam Y.C. (2004b), "Prediction of the deflection and residual stress in controlled cooling of hot-rolled steel beams including load and arbitrary support. Part II. Experimental validation and application", *Journal of Material Processing Technology*, 147, pp. 268-275.

Fischer F.D., Hinteregger E., Rammerstorfer F.G. (1991), "A computational study of the residual stress distribution in thermally loaded beams of cross-section on frictional support", in: P. Wrigers, W. Wagner (Eds.), *Non-linear Comp. Mechanics, State of the Art,* Springer, Berlin, pp. 737–750.

Fischer F.D., Hinteregger E., Rammerstorfer F.G. (1992), "the influence of frictional forces on the longitudinal stress distribution of thermally induced residual stresses in beams", in: H. Fujiwara, T. Abe, K. Tanaka (Eds), Proceedings of the Third International

Conference on Residual Stresses, Tokushima-shi, Japan, 1991, Residual Stresses. III. Science and Technology, v. 2, Elsevier, New York, London, pp. 1-16.

Hinteregge E., Fischer F.D., Rammerstorfer F.G. (1992), "The influence of frictional force on the longitudinal distribution of thermally induced residual stresses in beams", in: H. Fujiwara, T. Abe, K. Tanaka (Eds.), *Residual Stresses—III Science and Technology*, vol. 2, Elsevier, London, pp. 1278-1283.

Kusakabe T., Mihara Y. (1980), "Analysis of residual stresses in hot-rolled H shapes", *Trans. ISIJ*, v. 20, pp. 454-461.

Olden V., Thaulow C., Jjerpetj∅nn H., S∅rli K. and Osen V. (1998), "Numerical Simulation of temperature distribution and cooling rate in ship profiles during water spray cooling", Materials Science Forum, Vols. 284-286, Trans Tech Publications, Switzerland, pp. 385-392.

Marcelin J. L., Abouaf M. and Chenot J. L. (1986), "Analysis of residual stress in hot-rolled complex beams", *Computer Methods in Applied Mechanical and Engineering*, v. 56, pp. 1-16.

Nakata N., Yoshida H. (1995), "Influence of cooling uniformity at run-out table on strip flatness, Recent advances in heat transfer and micro-structure modelling for metal processing", in: Proceedings of the 1995ASME International Engineering Congress and Exposition, San Francisco, USA, Society of Mechanical Engineers, Materials Division, ASME, MD, pp. 67-77.

Takashi K., Nose J., Yoshida T., Wakimoto N. (1973), "Residual Stress in hot-rolled H-section steel", Nippon Kokan Technical Report, Overseas.

Yoshida H., Kataok K., Sasaki T., Tanaka T. (1982), "Analysis of deflection during cooling in rolled U-type sheet piles", Technology Laboratory Report, Kawasaki Iron Industry Pty. Ltd., 30 July.

Yoshida H. (1984a), "Analysis of residual stress in hot rolled H-beam", *Trans. ISIJ*, v. 24, pp. 401-407.

Yoshida H. (1984b), "Reduction of residual stress in hot rolled H-beam", *Trans. ISIJ*, v. 24, pp. 471–477.